



Research Article

Fuzzy adaptive variable impedance control on deformable shield of defecation smart care robot

Lingling Chen^{a,b,*}, Pengyue Lai^a, Yanglong Wang^a, Yuxin Dong^a^a School of Artificial Intelligence, Hebei University of Technology, Tianjin 300400, China^b Intelligent Rehabilitation Device and Detection Technology Engineering Research Centre of the Ministry of Education, Tianjin 300400, China

ARTICLE INFO

Article history:

Received 29 September 2024

Revised 25 December 2024

Accepted 14 January 2025

Available online 25 January 2025

Keywords:

Defecation smart care robot

Deformable shield

Human–robot contact force

Fuzzy adaptive variable impedance controller

ABSTRACT

Precise control of the contact force is crucial in the application of non-wearable defecation smart care (DSC) robot. A deformable shield equipped with a pressure sensing function is designed, with a bending angle that can be adjusted according to pressure feedback, thus enabling it to adapt to various body shapes. To improve the force tracking accuracy and prevent obvious force overshoot in the initial contact stage, a contact force control strategy based on fuzzy adaptive variable impedance is proposed. The proposed contact force control strategy achieves an average root-mean-square error of 0.024 and an average overshoot of 1.74%. Experimental results demonstrate that the designed deformable shield can fit the human body well, while the proposed control strategy enhances the contact force management and realizes the precise control of human–robot contact force.

© 2025 The Author(s). Published by Elsevier B.V. on behalf of Shandong University. This is an open access article under the CC BY-NC-ND license (<http://creativecommons.org/licenses/by-nc-nd/4.0/>).

1. Introduction

With the increasing aging population, the number of elderly individuals with bed-bound disabilities has grown [1]. The care of the bedridden elderly poses a higher challenge to other family members and social old-age service organizations, among which the defecation smart care (DSC) is one of the biggest challenges [2]. The DSC robots can assist bedridden elderly individuals with toileting needs in bed, provide cleaning and care, improve their quality of life and reduce the workload of nursing staff [3].

At present, the DSC robot products are primarily wearable, such as Automatic intelligent toilet care robot (Evercare, Japan) and Toilet care robot (Zuowei Technology Co., Ltd., China), as shown in Fig. 1(a), (b). These devices need to be wrapped around the body's private parts all day long, and have poor air permeability, which can cause a strong sense of confinement and discomfort.

In recent years, non-wearable DSC robots have attracted considerable attention due to their comfortable and unrestrictive design, for example, the Solaticare toileting intelligent care robot (Novamed Europe Co., UK) and the Longevity individuals care robot (Conbest Co., Ltd., China), with their shield structures illustrated in Fig. 1(c), (d). When the user needs to defecate, the bed under the hip opens and the shield rises from under the bed to fit snugly over the body's private parts. Once the body has been cleaned and cared for, the shield retracts back into the bed,

eliminating the need for prolonged contact with the body. This design does not restrict the elderly's movements, such as turning over in bed, thus providing greater comfort and freedom.

However, the bedridden elderly have different body types, especially most of the elderly are thin and weak [4]. At the same time, the existing non-wearable shield products have a simple structure, fixed bending angle and no pressure sensing function [5]. This results in gaps between the shield and the human body, does not fit the human body completely, thus making it easy for sewage to leak out and contaminate the bed during cleaning. Therefore, it is necessary to design a shield with a controllable bending angle to automatically match the user's shape.

Bedridden elderly individuals are fragile and cannot endure excessive contact force. When the shield contacts their bodies, insufficient contact force can result in the leakage of excrement, while excessive force will cause injury. Therefore, precise control of contact force is important to ensure the safety of human–machine interaction [6–9]. However, due to the innovative design of the shield, there are no directly applicable control methods available for reference. We conducted the survey on the control of contact force. Impedance control adjusts the robot's movements based on its interactions with the environment, enhancing the robot's flexibility during operation [10].

In impedance control, environmental stiffness and positioning play a critical role in influencing the system's contact force control performance [11–14]. In cases where the environmental stiffness is uncertain or the ambient position changes over time, the contact force control performance of fixed impedance parameter control becomes suboptimal. Therefore, researchers

* Corresponding author at: School of Artificial Intelligence, Hebei University of Technology, Tianjin 300400, China.

E-mail address: chenling@hebut.edu.cn (L. Chen).

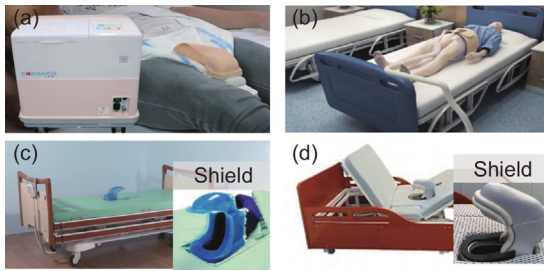


Fig. 1. Shield structure of DSC robot. (a) Evercare. (b) Zuowei. (c) Novamed. (d) Conbest.

have improved the impedance control strategy by optimizing impedance control parameters to adapt to unknown environments, thereby achieving the desired contact force. Li et al. [15] combined deep reinforcement learning with impedance control to realize robot massage tasks, accelerated agent exploration speed and improved learning efficiency of the contact force under complex conditions. Hamedani et al. [16] proposed a structured online adaptation mechanism that employs a wavelet neural network to adjust the impedance parameter, thereby enhancing the performance of force tracking. Li et al. [17] proposed a particle swarm optimization algorithm to adjust the impedance control parameters of the robot and improved the precision of force control. Zhang et al. [18] proposed a method for controlling variable impedance that relies on an observer. This approach utilized the observer to determine the variable impedance control rate for the robot, incorporating compensation for model disturbances, realized the contact force tracking and fulfilled the operational requirements for grinding thin-walled components. Beber et al. [19] proposed a method utilizing variable impedance control, which achieved tracking the target contact force throughout ultrasound procedures. While the varying constitutions of the elderly in bed and the differing degrees of skin deformation in response to stress must be taken into account, these factors make achieving better control challenging. Therefore, an adaptive variable impedance control strategy is designed to adjust impedance parameters in real-time during the control process, allowing the system to adapt to the complexities of human body contact and improve contact force tracking performance.

When the shield comes into contact with the human body, contact force overshoot situation may happen [20]. Given the frailty of bedridden elderly individuals, contact force overshoot need to be avoided to ensure their safety. Cao et al. [21] proposed an adaptive hybrid impedance control with a pre-PID tuner to reduce force overshoot at the initial contact stage and improve force tracking performance. Hammoud et al. [22] proposed a global optimal control strategy considering contact uncertainty to optimize the impedance curve and reduce the high impact force during the transition phase of contact. Quiñones et al. [23] used a Model Predictive Control (MPC) based approach to apply a controlled and customizable force impulse to a human. The above methods have excellent control effects and can effectively alleviate the problem of force overshoot. In comparison, fuzzy control offers a simpler structure and greater ease of implementation. Fuzzy-based variable impedance control strategies stand out for their simplicity, adaptability, and ease of implementation. They effectively reduce force overshoot and oscillations, ensuring smooth and precise force tracking in uncertain and dynamic environments, making them highly suitable for robotic applications [24–26]. Therefore, a fuzzy logic loop is proposed to optimize system parameters, reducing contact force overshoot and ensuring safe contact between the human and the shield.

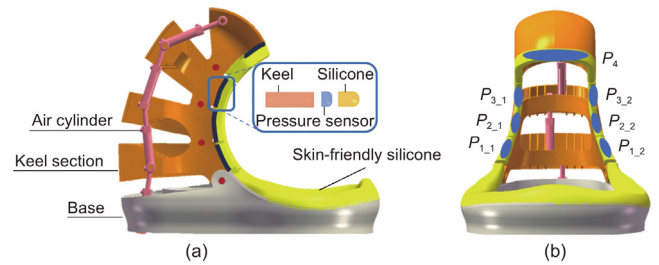


Fig. 2. Shield structure diagram. (a) Side cutaway view. (b) Front view.

To address the aforementioned challenges, a deformable multi-keel shield is designed and a force control algorithm is proposed, to ensure a safe and secure fit of the shield to the human body. The content of this paper is as follows:

- (1) A multi-keel deformable shield is designed with man-machine contact force sensing function;
- (2) An adaptive variable impedance control strategy is proposed to track the desired human-machine contact force;
- (3) A fuzzy logic loop is used to optimize the control parameters and solve the overshoot of system contact force.

2. Deformable shield design

2.1. Structure design

The contact surface between the shield and the human body is complex, which complicates the achievement of a close fit that creates a sealed cavity. The process of the shield fitting to the human body is similar to the process of the pangolin curling up. We designed a deformable shield inspired by the structure of pangolin scales. This shield primarily comprises a multi-section deformable keel, a pressure sensor, and a skin-friendly silicone lining as shown in Fig. 2.

We selected subjects of different body types for the experiment, with BMI ranging from 30.2 to 19.6. The subject with a BMI of 30.2 requires a bending angle of 15°, while the subject with a BMI of 19.6 requires 45°. To accommodate a wider range of body types, the shield bending angle range is set from 0°–60°. The bending angle ranges for each keel are 0°–20°, 0°–15°, 0°–15°, and 0°–10°.

Humans may experience a sense of being tightly wrapped when the DSC robot encloses their body. Human perception of force is subjective, so we refer to the contact force needs of some massage robots [27–29], and set the suitable contact force range to 3–8 N. The maximum contact force set in this study is 6N. To ensure it remains within the allowable range, the overshoot should not exceed 30%.

The deformable keel comprises four sequentially arranged keel sections, along with a base. These four sections are connected in series, with each adjacent pair linked by a single-rod double-acting cylinder. To enhance comfort, soft skin-friendly silicone lining is applied to the portions of the keel frame that come into contact with the human body. Additionally, pressure sensors are installed between the skin-friendly lining and the keel, creating a human-machine contact force sensing system.

As shown in Fig. 2(b), seven pressure sensors are sequentially positioned on the shield. A sensor is placed at the top of the shield, labeled P_4 , and the remaining six sensors are arranged on the left and right sides of the below three keel segments, labeled $P_{3,1}$, $P_{3,2}$, $P_{2,1}$, $P_{2,2}$, $P_{1,1}$, $P_{1,2}$. These sensors enable the shield to detect the contact force between the keel and the body, thereby reflecting the states of contact between the shield and the user. In order to ensure that the shield can be tightly fitted to the

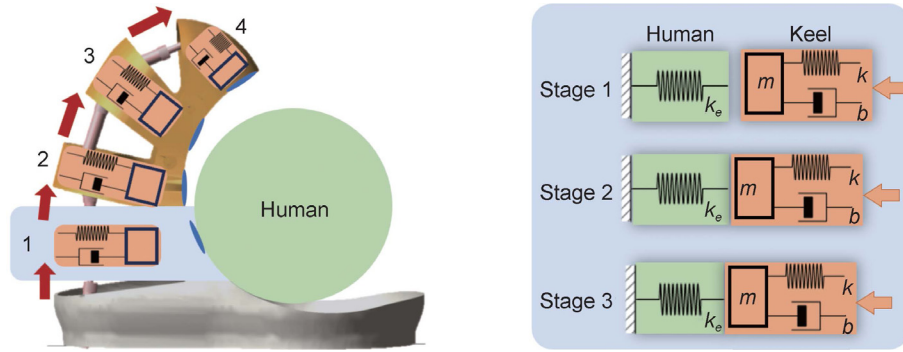


Fig. 3. Shield movement process.

human body, we chose the minimum pressure value as the force feedback corresponding to the keel.

When the user needs to defecate, the bed under the hip opens and the shield rises from under the bed to fit snugly over the body's private parts. The deformable shield is initially positioned upright before conforming to the human body. Once it fits the human form, the pressure sensing system of the shield can monitor the contact force between the edge of the shield and the body in real time. The four cylinders extend from bottom to top, thereby adjusting the bending angle of the shield to ensure a close fit against the human body. This structure can efficiently prevent sewage from splashing during defecation.

2.2. Contact process analysis

The process of the shield fitting to the human body is illustrated in Fig. 3. Initially, keel joint 1 moves towards the human body. When the keel joint 1 contacts the human body and the corresponding sensor ($\min |P_{1,1}, P_{1,2}|$) detects the target contact force, keel joint 1 ceases movement. Similarly, keel joints 2, 3, and 4 move sequentially according to the same principles until the shield is fully conformed to the human body and the sensors achieve the target contact force.

We use the contact process between keel joint 1 and the human body as a case example to model the contact force applied by the shield on the human body. The shield is modeled as a second-order system consisting of mass, spring, and damper components, while the human skin tissue is modeled as a first-order spring. It is assumed that the contact force is directly proportional to the depth of the shield's embedding in the environment. The parameters k_e , m , b , and k denote the environmental stiffness, the mass, damping, and stiffness of the shield keel joint, respectively.

The contact process is divided into three stages:

- (1) there is no contact between the shield and the human body, resulting in the absence of contact force;
- (2) a collision occurs between the shield and the human body;
- (3) the contact force between the shield and the human body reaches a stable state.

This paper primarily examines the contact force during the latter two stages, focusing on enhancing the performance of the force control strategy to achieve compliance transition and improve force tracking accuracy in the stable contact stage.

3. Fuzzy adaptive variable impedance control of shield

A Fuzzy Adaptive Variable Impedance Control (FAVIC) strategy is proposed to realize the tight fit between the shield and the human body, as shown in Fig. 4. The control strategy adds adaptive variable impedance and a fuzzy controller to the force feedback loop of impedance control. Set $\mathbf{f}_{di} = [f_{d1}, f_{d2}, f_{d3}, f_{d4}]^T$ represents the expected contact force of the four keel joints closely

fitting to the human body. Similarly $\mathbf{x}_{ei} = [x_{e1}, x_{e2}, x_{e3}, x_{e4}]^T$ and $\Delta \mathbf{x}_{ei} = [\Delta x_{e1}, \Delta x_{e2}, \Delta x_{e3}, \Delta x_{e4}]^T$ respectively represent the reference trajectory of the four keel joints and the corrected trajectory obtained according to the contact force error, $\boldsymbol{\theta}_i = [\theta_1, \theta_2, \theta_3, \theta_4]^T$ represents the actual angle of the four keel joints.

3.1. Adaptive impedance control

During the process of fitting the shield to the human body, the complex dynamic changes in human skin that the human body is stressed, along with the difficulty in directly obtaining stiffness information from the skin's surface, render traditional constant impedance control strategies inadequate for adapting to these intricate situations in a timely manner. Consequently, the accuracy of force tracking is compromised.

To address this issue, a variable impedance control strategy is proposed, which adjusts the damping and stiffness coefficients in real time according to the force tracking error. By continuously monitoring the deviation in force tracking, the impedance coefficients are dynamically modified to sustain the steady-state performance of the control system.

The contact force exerted between the shield and the human body can be simplified as

$$\mathbf{f}_e = k_e (\mathbf{x}_e - \mathbf{x}_c) \quad (1)$$

where \mathbf{x}_e is the environmental position, \mathbf{x}_c is the shield position, and k_e is the environmental stiffness. The position disturbance caused by the contact force is $\mathbf{e} = \mathbf{x}_c - \mathbf{x}_e$.

The contact force error is $\Delta \mathbf{f} = \mathbf{f}_e - \mathbf{f}_d$, where \mathbf{f}_d represents the expected contact force.

The contact force error and displacement error are brought into the constant impedance equation $g(s) = 1/(ms^2 + bs + k)$, and the new impedance equation is:

$$\Delta \mathbf{f} = m(\ddot{\mathbf{x}}_c - \ddot{\mathbf{x}}_e) + b(\dot{\mathbf{x}}_c - \dot{\mathbf{x}}_e) + k(\mathbf{x}_c - \mathbf{x}_e) \quad (2)$$

When the contact surface is a complex dynamic case, \mathbf{x}_e is unknown, and the environmental position estimate should not be zero, that is $\dot{\mathbf{x}}_e \neq 0$, or $\ddot{\mathbf{x}}_e \neq 0$. Assuming the estimated environmental position $\hat{\mathbf{x}}_e = \mathbf{x}_e - \delta \mathbf{x}_e$, the position error is $\hat{\mathbf{e}} = \mathbf{e} + \delta \mathbf{x}_e$, substituting $\hat{\mathbf{e}}$ for \mathbf{e} by Eq. (2), the result is:

$$\Delta \mathbf{f} = m\ddot{\hat{\mathbf{e}}} + b\dot{\hat{\mathbf{e}}} + k\hat{\mathbf{e}} = m(\ddot{\mathbf{e}} + \delta\ddot{\mathbf{x}}_e) + b(\dot{\mathbf{e}} + \delta\dot{\mathbf{x}}_e) + k(\mathbf{e} + \delta\mathbf{x}_e) \quad (3)$$

In order to ensure steady-state force tracking error is zero ($\Delta \mathbf{f}_{ss} = 0$), the adaptive impedance parameter is designed to compensate the time-varying error, while considering the stability of the system, the adaptive impedance parameter is compensated. Δb and Δk are used for dynamic compensation $m\delta\ddot{\mathbf{x}}_e + b\delta\dot{\mathbf{x}}_e + k\delta\mathbf{x}_e$, so the following adaptive variable impedance control

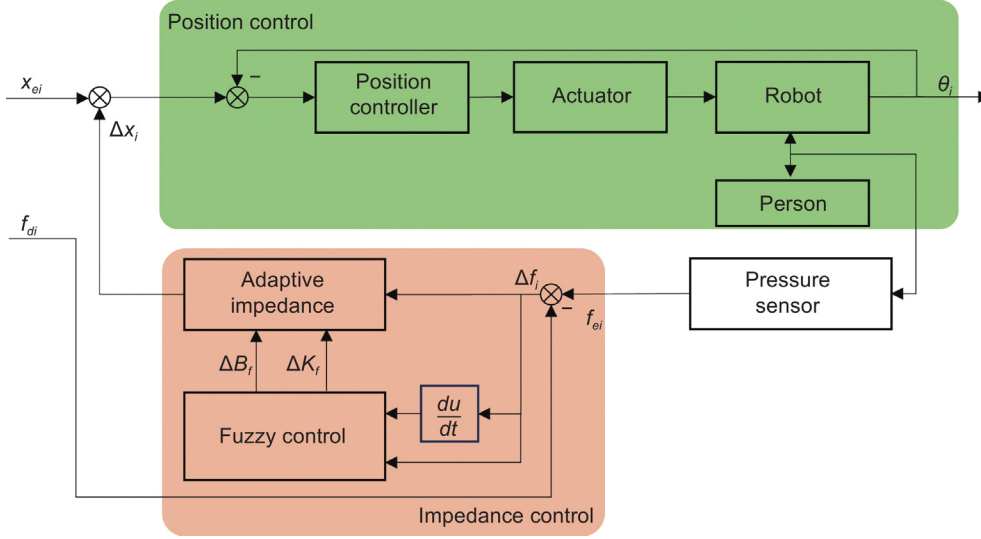


Fig. 4. Fuzzy adaptive variable impedance control framework based on the shield.

rate is proposed:

$$\Delta \mathbf{f} = m\ddot{\mathbf{e}}(t) + (b + \Delta b)\dot{\mathbf{e}}(t) + (k + \Delta k)\mathbf{e}(t) \quad (4)$$

The adaptive rate is as follows:

$$\begin{cases} \Delta b = b\varphi_b(t)/\dot{\mathbf{e}} \\ \varphi_b(t) = \varphi_b(t - \lambda) + \sigma [\mathbf{f}_d(t - \lambda) - \mathbf{f}_e(t - \lambda)]/b \\ \Delta k = k\varphi_k(t)/\mathbf{e} \\ \varphi_k(t) = \varphi_k(t - \lambda) + \eta [\mathbf{f}_d(t - \lambda) - \mathbf{f}_e(t - \lambda)]/k \end{cases} \quad (5)$$

where λ is the sampling rate, σ and η are the update rate of damping coefficient and stiffness coefficient respectively. $\varphi_b(t)$ and $\varphi_k(t)$ correspond to the real-time adjustments of the damping and stiffness coefficients based on the force error data.

3.2. Fuzzy variable impedance control

During contact between the shield and the human body, the collision characteristics can result in a sharp rise in the contact force, leading to the issue of contact force overshoot, which can easily lead to human injury. This overshoot problem can be effectively mitigated by adjusting the parameters of the impedance controller. Fuzzy control is characterized by its simple structure, strong anti-interference capabilities, and good robustness, making it suitable for systems where obtaining accurate dynamic models is challenging. Therefore, a fuzzy logic loop is introduced to adjust the k and b instantaneously.

A two-input two-output fuzzy controller is designed to adjust the stiffness coefficient k and damping coefficient b in real time. The input variables of the fuzzy control loop are contact force error δ_f and contact force error change rate δ_{fc} , and the output variables are stiffness coefficient correction and damping coefficient correction. The contact force error δ_f and its rate of change δ_{fc} are defined as follows:

$$\begin{cases} \delta_f = \mathbf{f}_e - \mathbf{f}_d \\ \delta_{fc} = (\mathbf{f}_e - \mathbf{f}_d)/\Delta t \end{cases} \quad (6)$$

The outputs Δb_f and Δk_f of the fuzzy controller are linearly superimposed on the outputs Δb and Δk of the adaptive impedance controller, respectively, as follows:

$$\begin{cases} b = \Delta b_f + \Delta b \\ k = \Delta k_f + \Delta k \end{cases} \quad (7)$$

The experimental results show that better results can be obtained by using 7 grades {NB, NM, NS, Z, PS, PM, PB} to describe the state of input and output variables. Gaussian membership function is selected. Membership functions for δ_f , δ_{fc} , Δb_f and Δk_f are shown in Fig. 5.

When the shield is in contact with the human body, if the contact force is too small, it cannot be effectively fitted, and if the contact force is too large, it will cause damage to the body. Therefore, the design of the fuzzy rule should follow these principles:

(1) If the input δ_f and δ_{fc} are positive, it indicates that the force error tends to increase and the contact force exceeds the expected force. In order to protect the patient, the shield should have lower rigidity. In this case, the fuzzy controller outputs a larger b and a smaller k .

(2) If the input δ_f and δ_{fc} are negative, it indicates that the force error tends to decrease and the contact force is below the expected force. In order to better fit the shield and the human body, the shield should have greater rigidity. In this case, the fuzzy controller outputs a smaller b and a larger k .

We use the Mamdani method for fuzzy reasoning and weighted average method for defuzzification. The fuzzy logic results of output Δb_f and Δk_f of the fuzzy controller are shown in Fig. 6.

4. Simulation and experiment

4.1. Evaluation method

The Root Mean Square Error (RMSE) and Overshoot are used to compare the performance of different control strategies. Lower values of RMSE and Overshoot indicate higher force tracking accuracy in the system and reduced overshoot during the initial contact. RMSE and Overshoot are defined as follows:

$$RMSE = \sqrt{\frac{1}{n} \sum_{i=1}^n (F_{actual,i} - F_{target,i})^2} \quad (8)$$

$$Overshoot = \frac{F_{max} - F_{ss}}{F_{ss}} \times 100\% \quad (9)$$

where n represents the total number of data points, $F_{actual,i}$ is the actual contact force, and $F_{target,i}$ is the target contact force, F_{max} is the maximum value of the system response, F_{ss} is the steady-state value of the system.

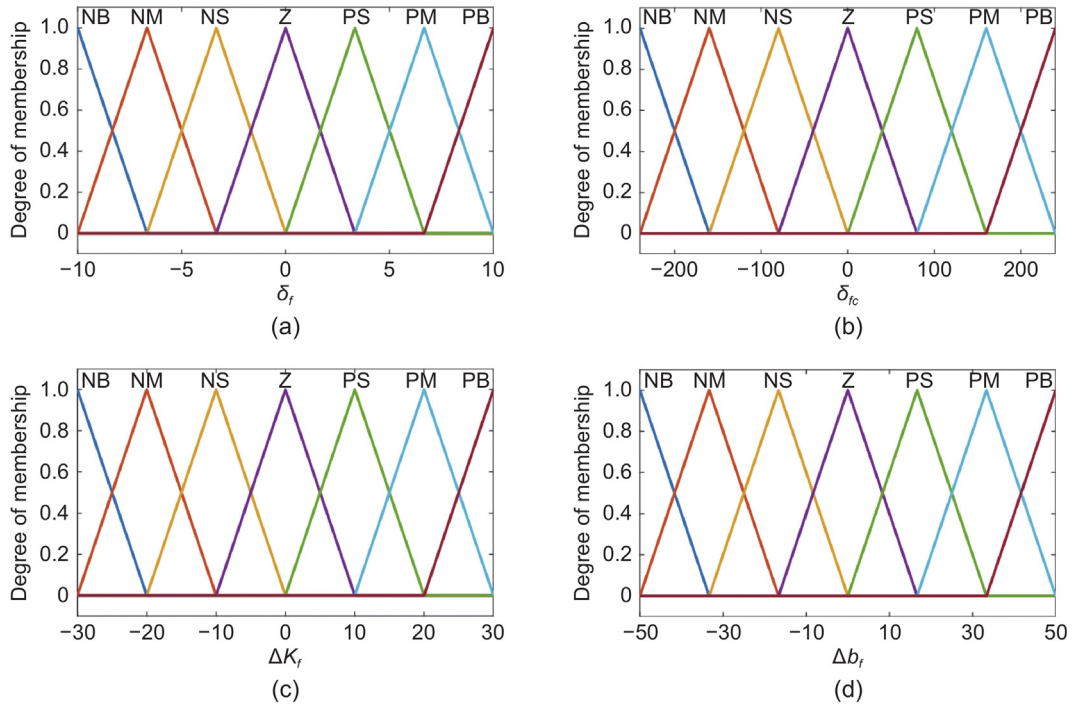


Fig. 5. Membership function. (a) δ_f . (b) δ_{fc} . (c) Δk_f . (d) Δb_f .

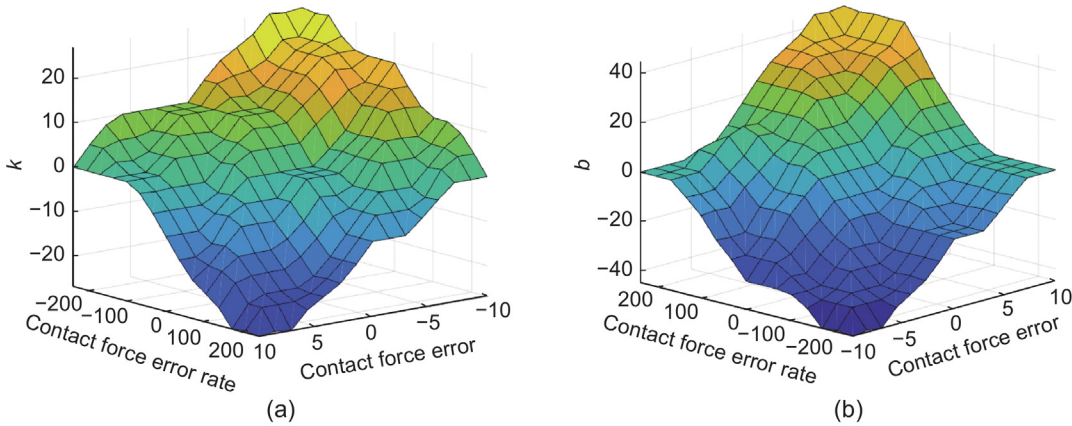


Fig. 6. Fuzzy variable impedance controller. (a) Fuzzy control surface of k . (b) Fuzzy control surface of b .

4.2. Simulation results

A simulation experiment is conducted to verify the effectiveness of the proposed strategy, on the contact force control system within the MATLAB (2023b)/Simulink environment. We evaluated and compared the constant force tracking algorithm of Constant Impedance Control (CIC), Adaptive Variable Impedance Control (AVIC), and the FAVIC introduced in this paper. For the purpose of testing and comparison, the following simulation test focuses on one direction. Detailed parameter settings are shown in Table 1. The sampling period for the simulation is set at 5 ms.

Assuming that the contact environment is a plane and the stiffness of the environment is unknown, the system tracks a constant force. The results of the contact force response for each keel section, along with the displacement curve of the keel section, are presented in Fig. 7. It is evident from the figure that during the process of the shield being fitted to the human body, each keel section generates contact force with the human body

sequentially, indicating that the shield can achieve a close fit. In comparison, CIC exhibits a larger force tracking error and a significant force overshoot during the initial stage of contact. While AVIC shows a smaller force tracking error, it also experiences a force overshoot at the beginning of contact, as illustrated in Fig. 7(a).

From the perspective of quantitative analysis, the results are illustrated in Fig. 8. The average overshoot of the CIC and AVIC algorithms is 28.468% and 19.463%, respectively, while the FAVIC algorithm achieves an average overshoot of just 2.122%. This demonstrates that FAVIC effectively mitigates the overshoot problem during the early contact stage and satisfies the design requirement of keeping the overshoot below 30%. Additionally, the mean RMSE values for CIC and AVIC are 0.548 and 0.137, respectively, compared to 0.6903 for FAVIC. These results indicate that FAVIC achieves precise tracking of the desired force and effectively addresses the force-tracking problem.

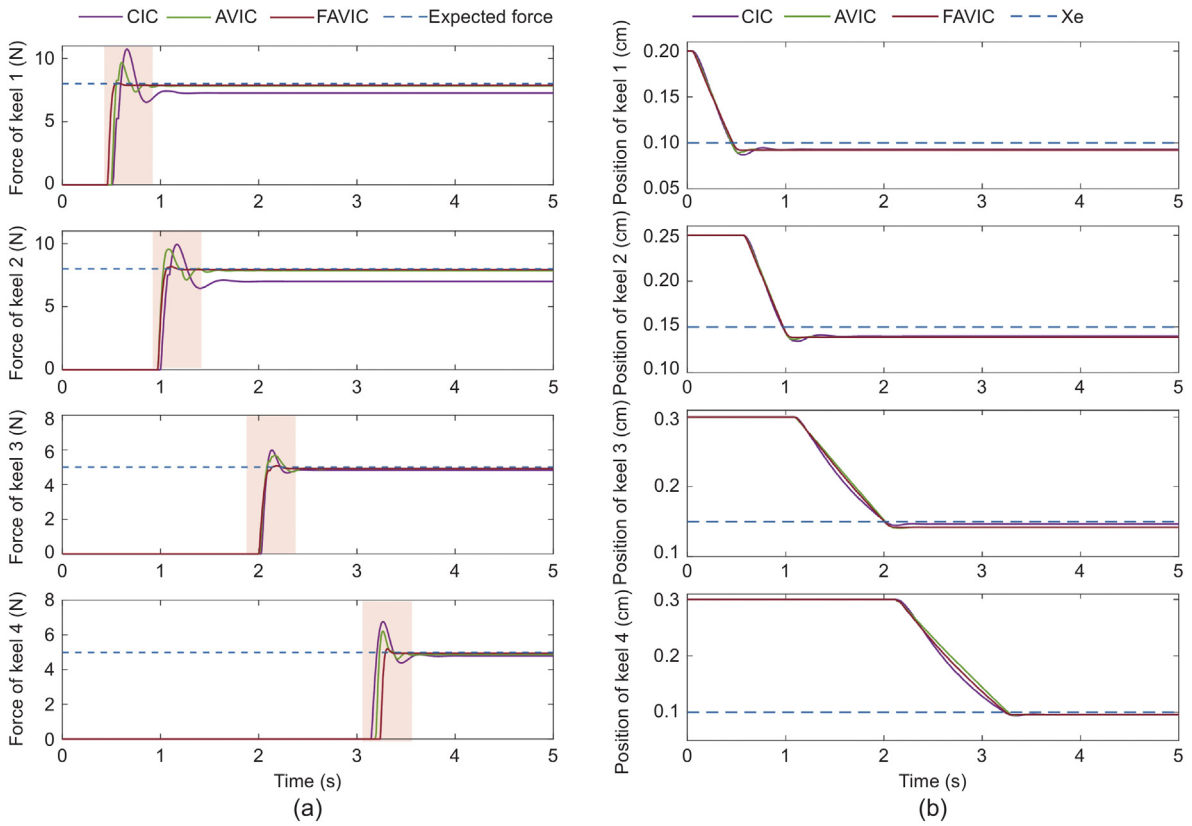


Fig. 7. Simulation results of different control strategy. (a) Force-tracking curve. (b) Position curve.

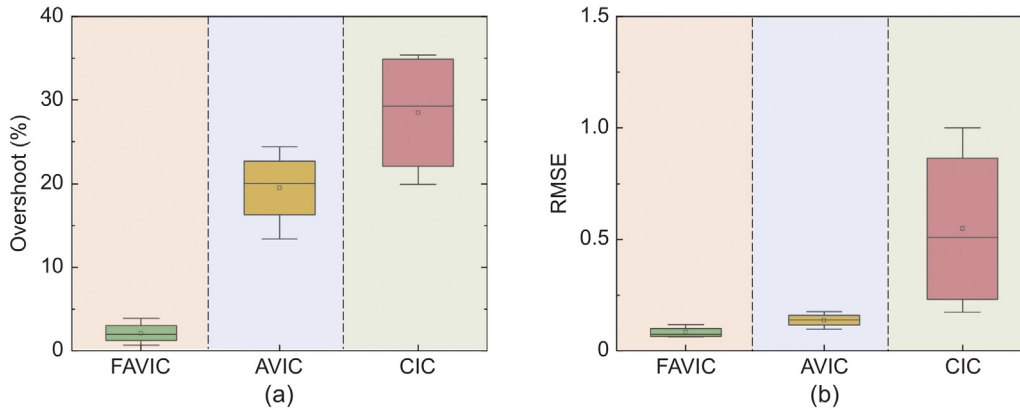


Fig. 8. Quantitative evaluation of Simulation results. (a) Overshoot. (b) RMSE.

4.3. System composition

We use PID controller as the impedance control inner ring to control the position of the cylinder. The maximum displacement of the cylinder is 45 mm, the PID parameters are $k_p = 3.50$, $k_i = 0.01$, $k_d = 0.01$ respectively. The control performance is shown in Fig. 9(a). The position control accuracy of the cylinder is ± 1 mm, which meets the control requirements.

The sensor calibration was conducted over a range of 10 g to 1.5 kg. The experimental results, as presented in the figure, indicate a linear relationship between the applied pressure and the sensor output. A linear fit yielded the equation $y = 195.298x + 837.397$ with a coefficient of determination (R^2) of 0.977.

A bending response test of the shield was conducted by sequentially extending each joint to its maximum range. The bending angle of the shield was measured using an angle sensor.

The experimental results, as shown in Fig. 9(c), indicate that the response time is between 1.5 to 2 s, which adequately meets the practical requirements of the defecation care.

The hardware system composition of the deformable shield is illustrated in Fig. 10, and includes the following components: a STM32 control board (STM32F103ZE, DC 5V), a voltage amplification module, a five-position three-way proportional directional valve (MPYE-5-1/8-LF-010-B, FESTO, DC 24V), a solenoid valve group (0520D, VALVE, DC 24V), an air pump (DC 24V), a pressure sensor (PR-C7.6-LT, DC 5V), and a self-developed single-rod double-acting cylinder. To ensure the device can deliver maximum contact force and overcome external resistance during the experiment, we selected an air pump capable of providing a maximum atmospheric pressure of 120 kPa, which allows it to generate a maximum contact force of 12 N. The control board receives data from the pressure sensor and calculates the output control

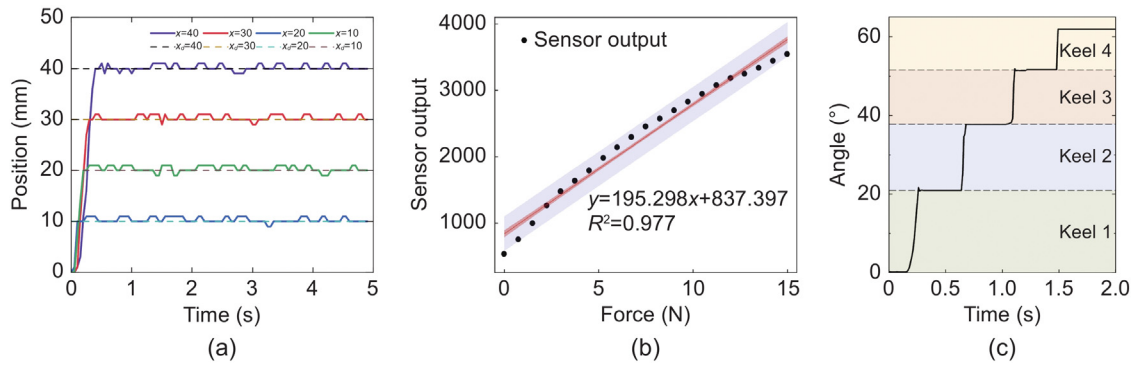


Fig. 9. Performance experiment. (a) Cylinder control accuracy. (b) Pressure sensor calibration. (c) Response speed of the bending action.

Table 1
Control parameter.

Method	Symbol	Description	Value	Units
CIC	m	inertia	0.5	Nm/(rad s ²)
	b	damping	80	Nm/(rad s)
	k	stiffness	50	Nm/rad
AVIC	m_0	inertia base values	0.5	Nm/(rad s ²)
	b_0	damping base values	80	Nm/(rad s)
	k_0	Stiffness base values	50	Nm/rad
	λ	Sampling rate	0.01	–
	σ	Damping renewal rate	0.5	–
	η	Stiffness renewal rate	0.2	–
FAVIC	m_0	inertia base values	0.5	Nm/(rad s ²)
	b_0	damping base values	80	Nm/(rad s)
	k_0	Stiffness base values	50	Nm/rad
	λ	Sampling rate	0.01	–
	σ	Damping renewal rate	0.5	–
	η	Stiffness renewal rate	0.2	–
	b_l	Damped output limit	30	–
k_l	Stiffness output limit	50	–	

signal, which is then transmitted to the five-position three-way proportional valve via the voltage amplification module. The control board controls the valve opening of the proportional valve, thereby regulating the air intake of the cylinder to manage its speed and direction of travel. Additionally, the STM32 control board governs the opening and closing of the solenoid valve group based on the collected pressure data, enabling selective control over the start and stop operations of the four cylinders.

4.4. Experimental results

To validate the simulation study, physical experiments are conducted to assess the feasibility of the proposed algorithm. As the pose of the model illustrated in Fig. 11, the subjects are instructed to sit on the deformable shield designed in this study and participate in the experiment. The process of the shield conforming to the human body is depicted in Fig. 12. The sections of the shield frame are bent and adjusted to fit the human body from the bottom to the top. When the corresponding sensor value reaches the desired force, the next keel section begins to conform to the human body. In this section, the proposed control strategy is applied to conduct experiments on ten healthy subjects, and the experimental results are presented. All individuals voluntarily agreed to participate in the experiment after obtaining ethical approval from the Ethics Committee of Xuanwu Hospital, Capital Medical University. The information of the subjects is shown in Table 2.

The results of the experiment are illustrated in Fig. 13. Initially, the shield transitions from free space to the human. Once the shield contacts the human body surface, the actual contact

Table 2
Subjects' detailed information.

	Gender	Age	Weight/kg	Height/cm	BMI
Person1	Male	27	92.5	175	30.2
Person2	Male	24	70	175	22.8
Person3	Female	24	63	181	19.4
Person4	Male	23	75	176	24.2
Person5	Male	25	71	173	23.7
Person6	Male	24	70	175	22.8
Person7	Male	24	69	170	23.9
Person8	Male	23	60	170	20.8
Person9	Male	25	60	175	19.6
Person10	Male	25	93	178	29.4

force can smoothly track the expected contact force after a brief adjustment period. The contact force error in the steady contact phase of the CIC is significant, and its tracking performance of the expected force is suboptimal. In contrast, the AVIC demonstrates superior steady-state force tracking; however, it exhibits a force overshoot phenomenon during the initial phase of contact. On the other hand, the FAVIC does not generate an impact during the early contact phase and maintains a minimal steady-state error. For subjects with BMI of 30.2 and 19.4, the contact force response is illustrated in Fig. 13(a), (b). The fitting process takes approximately 1.0 to 2.0 s, which aligns with the time required to accommodate the human body prior to defecation.

We use quantitative evaluation to analyze the effectiveness of different control strategies. As illustrated in Fig. 14, the performance of the CIC algorithm in each joint is inferior to that of the other two algorithms (AVIC, FAVIC), the mean RMSE is 0.147, with an average overshoot of 15.307%, indicating the largest steady-state error and overshoot. In comparison, the AVIC algorithm achieves an average RMSE of 0.102 and an average overshoot of 8.984%, demonstrating improvements in both steady-state error and overshoot. Furthermore, the mean control accuracy of the FAVIC algorithm is 0.024, which is lower than that of CIC, and its average overshoot is 1.74%, significantly lower than that of both CIC and AVIC. These results indicate that the FAVIC algorithm exhibits superior control performance, ensuring high force-tracking accuracy while avoiding impact forces.

5. Conclusions

This paper designs a deformable shield of the non-wearable DSC robot and proposes a contact force control strategy for different people. A deformable multi-keel joint shield equipped with pressure sensing capabilities is designed to accommodate users of varying body shapes and conform to the complex contact surfaces of the human body. A dynamic physical characteristic model of the interaction between the shield and the human body

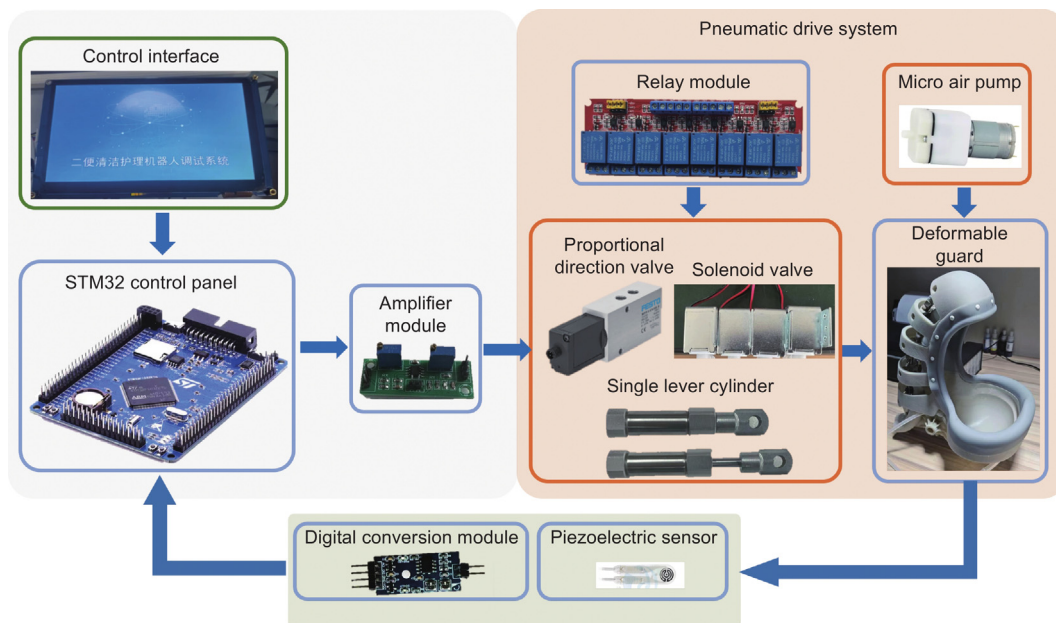


Fig. 10. System hardware composition.



Fig. 11. Shield prototype diagram. (a) Side view. (b) Front view.

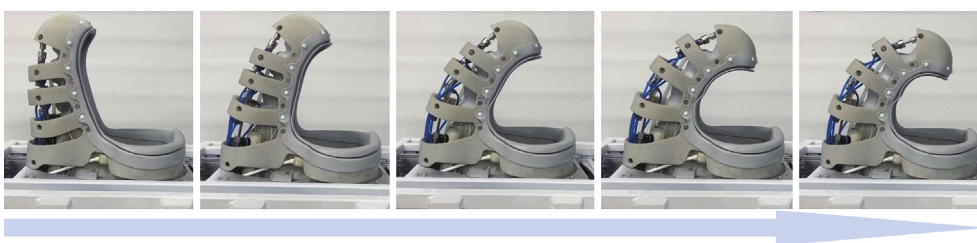


Fig. 12. Shield bending process.

is established, and the motion characteristics of the shield are analyzed. Building upon traditional constant impedance control, a variable impedance control strategy is proposed that maintains excellent force tracking accuracy, even when interacting with unknown human skin surfaces. To address the issue of force overshoot in the initial contact phase of the variable impedance control strategy, a fuzzy adaptive variable impedance control strategy is introduced to mitigate the impact force by adjusting the impedance parameters. The simulation results indicate that the FAVIC demonstrates effective contact force control performance, whereas the AVIC exhibits overshoot characteristics and the CIC shows significant force deviation. Furthermore, FAVIC

achieves smooth contact force tracking performance during experiments involving the fitting of the shield to the human body, ensuring both accurate contact force tracking and the resolution of contact force overshoot issues. The FAVIC effectively adapts to complex variations in the contact environment, ensuring contact force accuracy and minimizing force overshoot. This enhances the comfort and safety of human-machine interactions, making it highly significant for elderly care applications.

The next stage of research will focus on improvements in the following areas: (1) The current actuator utilizes a cylinder, which poses challenges for precise control. Future work will aim to enhance the actuator design for improved accuracy. (2) The DSC robot is designed to remain hidden under the bed when not in

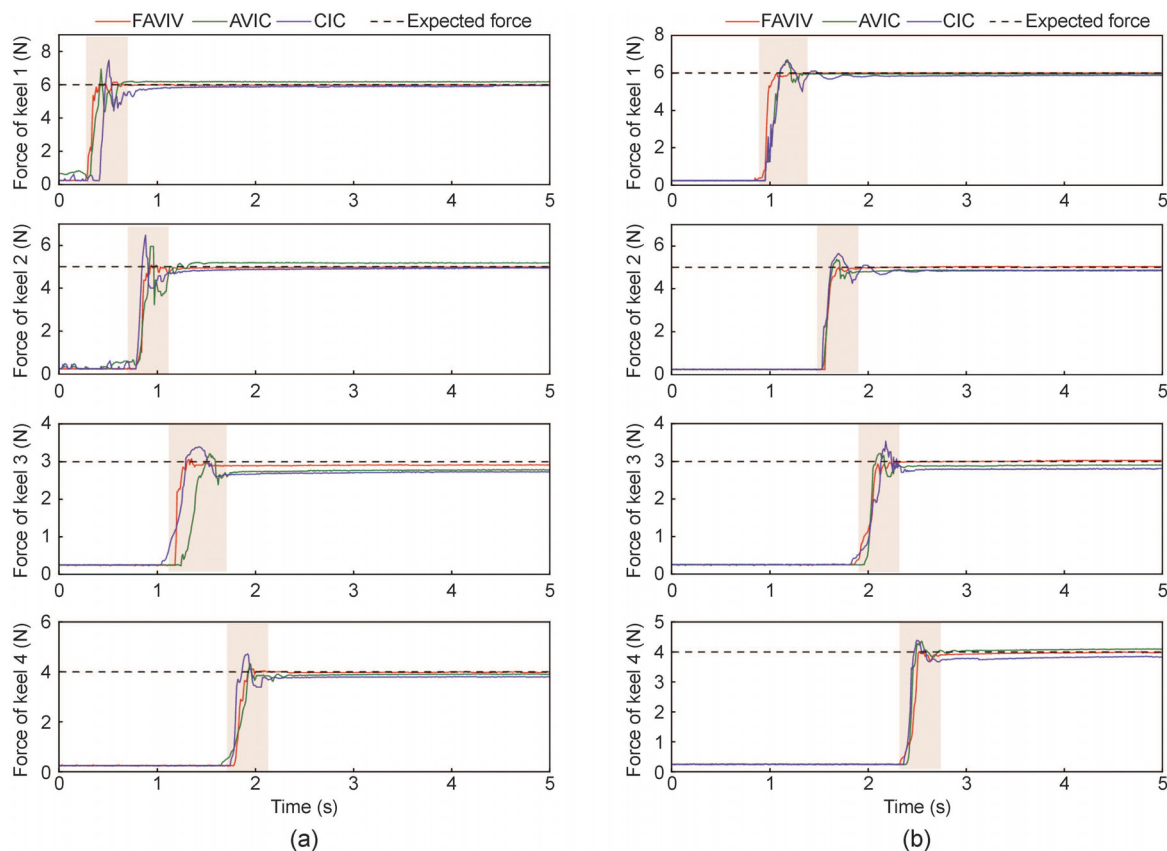


Fig. 13. Experimental results of different control strategy. (a) Person1. (b) Person3.

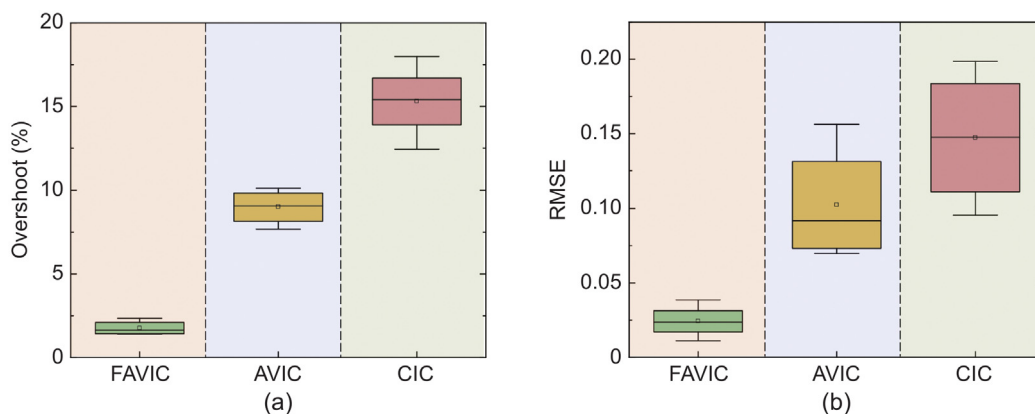


Fig. 14. Quantitative evaluation of experimental results. (a) Overshoot. (b) RMSE.

use. This study primarily addresses the fitting mechanism with the user and does not delve into the control aspects of lifting, alignment, or the forward and backward adjustments of the hip. These aspects will be the primary focus of subsequent research.

CRediT authorship contribution statement

Lingling Chen: Writing – review & editing, Resources, Project administration, Methodology, Investigation, Funding acquisition, Formal analysis, Data curation, Conceptualization. **Pengyue Lai:** Writing – original draft, Supervision, Software. **Yanglong Wang:** Validation. **Yuxin Dong:** Visualization.

Ethics approval

This work was approved by the Ethics Committee of Xuanwu Hospital, Capital Medical University (ChiCTR2400092918).

Declaration of competing interest

The authors declare that they have no known competing financial interests or personal relationships that could have appeared to influence the work reported in this paper.

Acknowledgments

This work was supported by grants from the National Key R and D Program of China (2022YFB4703300).

Appendix A. Supplementary data

Supplementary material related to this article can be found online at <https://doi.org/10.1016/j.birob.2025.100214>.

References

- [1] B. Sathian, E. Van Teijlingen, P. Simkhada, et al., Evidence-based approaches in aging and public health, *Front. Public Heal.* 12 (2024) 1391432.
- [2] C. Shaw, A. Wagg, Urinary and faecal incontinence in older adults, *Medicine* 49 (1) (2021) 44–50.
- [3] W. Wang, W. Ren, M. Li, et al., A survey on the use of intelligent physical service robots for elderly or disabled bedridden people at home, *Int. J. Crowd Sci.* 8 (2) (2024) 88–94.
- [4] H.T. Kohara, M. Ikeda, K. Yokotani, et al., Skin characteristics of sites predisposed to pressure ulcers among bedridden elderly patients in Japan, *Open J. Nurs.* 11 (6) (2021) 497–512.
- [5] S. Sang, W. Lu, F. Yuan, et al., Inner bowl of operating head of nursing machine, and nursing machine, 2018, U.S. Patent 10 105, 271.
- [6] J. Peng, A. Kimmig, D. Wang, et al., Intention recognition-based human-machine interaction for mixed flow assembly, *J. Manuf. Syst.* 72 (2024) 229–244.
- [7] S. Peng, M. Yu, X. Geng, et al., A lightweight exoskeleton force feedback glove, *Actuators* 12 (5) (2023) 199.
- [8] X. Liang, Y. Yan, W. Wang, et al., Adaptive human-robot interaction torque estimation with high accuracy and strong tracking ability for a lower limb rehabilitation robot, *IEEE/ASME Trans. Mechatronics* 29 (6) (2024) 4814–4825.
- [9] X. Liang, G. He, T. Su, et al., Finite-time observer-based variable impedance control of cable-driven continuum manipulators, *IEEE Trans. Hum. Mach. Syst.* 52 (1) (2021) 26–40.
- [10] N. Hogan, Impedance control of industrial robots, *Robot. Comput.-Integr. Manuf.* 1 (1) (1984) 97–113.
- [11] A.C. Huang, K.J. Lee, W.L. Du, et al., Contact force cancelation in robot impedance control by target impedance modification, *Robotica* 41 (6) (2023) 1733–1748.
- [12] H.F.N. Al-Shuka, S. Leonhardt, W.H. Zhu, et al., Active impedance control of bioinspired motion robotic manipulators: An overview, *Appl. Bionics Biomech.* 2018 (1) (2018) 8203054.
- [13] H. Hu, X. Wang, L. Chen, Impedance with finite-time control scheme for robot-environment interaction, *Math. Probl. Eng.* 2020 (1) (2020) 2796590.
- [14] Z. Zhu, H. Zhang, G. Liu, et al., Adaptive variable impedance force/position hybrid control for large surface polishing, *Ind. Rob.* 51 (5) (2024) 747–760.
- [15] Z. Li, C. Zeng, Z. Deng, et al., Learning variable impedance control for robotic massage with deep reinforcement learning: A novel learning framework, *IEEE Syst. Man Cybern. Mag.* 10 (1) (2024) 17–27.
- [16] M.H. Hamedani, H. Sadeghian, M. Zekri, et al., Intelligent impedance control using wavelet neural network for dynamic contact force tracking in unknown varying environments, *Control Eng. Pract.* 113 (2021) 104840.
- [17] L. Li, T. Huang, C. Pan, et al., Impedance control for force tracking of a dual-arm cooperative robot based on particle swarm optimization, *Ind. Rob.* 51 (3) (2024) 436–445.
- [18] Y. Zhang, X. Zhao, Y. Chen, et al., Observer-based variable impedance control using moving horizon estimation for robot machining thin-walled workpieces, *IEEE Trans. Ind. Electron.* 71 (6) (2023) 5972–5982.
- [19] L. Beber, E. Lamon, D. Nardi, et al., A passive variable impedance control strategy with viscoelastic parameters estimation of soft tissues for safe ultrasonography, in: 2024 IEEE Int. Conf. Robot. Autom., ICRA, 2024, pp. 1298–1304.
- [20] Z. Li, H. Wang, H. Zhao, et al., Force impact suppression of contact transition state in robot grinding and polishing of industrial blades, *Proc. Inst. Mech. Eng. C* 236 (236) (2022) 7387–7397.
- [21] H. Cao, Y. He, X. Chen, et al., Smooth adaptive hybrid impedance control for robotic contact force tracking in dynamic environments, *Ind. Rob.* 47 (2) (2020) 231–242.
- [22] B. Hammoud, M. Khadiv, L. Righetti, Impedance optimization for uncertain contact interactions through risk sensitive optimal control, *IEEE Robot. Autom. Lett.* 6 (3) (2021) 4766–4773.
- [23] D.P. Quiñones, M. Paterna, C. De Benedictis, et al., Contact force regulation in physical human-machine interaction based on model predictive control, *Robotica* 41 (11) (2023) 3409–3425.
- [24] K. Sun, J. Qiu, H.R. Karimi, et al., Event-triggered robust fuzzy adaptive finite-time control of nonlinear systems with prescribed performance, *IEEE Trans. Fuzzy Syst.* 29 (6) (2020) 1460–1471.
- [25] D. Kong, Q. Huang, Impedance force control of manipulator based on variable universe fuzzy control, *Actuators* 12 (8) (2023) 305.
- [26] Y. Guo, J. Peng, S. Ding, et al., Fuzzy-based variable impedance control of uncertain robot manipulator in the flexible environment: A nonlinear force contact model-based approach, *J. Intell. Fuzzy Syst* (2023) Preprint: 1–15.
- [27] Q. Xu, Z. Deng, C. Zeng, et al., Toward automatic robotic massage based on interactive trajectory planning and control, *Complex Intell. Syst.* 10 (3) (2024) 4397–4407.
- [28] J. Zhai, R. Li, Z. Su, Friction and deformation behavior of human skin during robotic sliding massage operation, *J. Bionic Eng.* (2024) 1–13.
- [29] F. Wang, C. Chen, C. Di, et al., Compliance control of a rehabilitation massage robot in dynamic scenes, *J. Phys. Conf. Ser.* 2816 (1) (2024) 012103.